RAA 2014 Vol. **14** No. **10**, 1221–1233 doi: 10.1088/1674–4527/14/10/002
http://www.raa-journal.org *http://www.iop.org/journals/raa*

Research in Astronomy and Astrophysics

Four new observational $H(z)$ data from luminous red galaxies in the Sloan Digital Sky Survey data release seven *

Cong Zhang[1], Han Zhang[1], Shuo Yuan[1], Siqi Liu[1], Tong-Jie Zhang[1] and Yan-Chun Sun[1]

Department of Astronomy, Beijing Normal University, Beijing 100875, China; *tjzhang@bnu.edu.cn*

Received 2013 May 24; accepted 2014 May 8

Abstract By adopting the differential age method, we select 17 832 luminous red galaxies from the Sloan Digital Sky Survey Data Release Seven covering redshift $0 < z < 0.4$ to measure the Hubble parameter. Using the full spectrum fitting package `UlySS`, these spectra are reduced with single stellar population models and optimal age information from our selected sample is derived. With the decreasing age-redshift relation, four new observational $H(z)$ data (OHD) points are obtained, which are $H(z) = 69.0 \pm 19.6$ km s^{-1} Mpc^{-1} at $z = 0.07$, $H(z) = 68.6 \pm 26.2$ km s^{-1} Mpc^{-1} at $z = 0.12$, $H(z)$=72.9 ± 29.6 km s^{-1} Mpc^{-1} at $z = 0.2$ and $H(z)$=88.8 ± 36.6 km s^{-1} Mpc^{-1} at $z = 0.28$, respectively. Combined with 21 other available OHD data points, the performance of the constraint on both flat and non-flat ΛCDM models is presented.

Key words: cosmology: cosmological parameters — cosmology: observations — galaxies: evolution

1 INTRODUCTION

A variety of cosmological observations are used for a better quantitative understanding of the expansion of the Universe, for example mapping the cosmic microwave background (CMB) anisotropies (Spergel et al. 2007; Komatsu et al. 2011), measurement of baryon acoustic oscillation (BAO) peaks (Eisenstein et al. 2005; Percival et al. 2010), and measurements of "standard candles" such as the redshift-distance relationship exhibited by type Ia supernovae (SNIa; Riess et al. 1998; Hicken et al. 2009) and gamma-ray bursts (GRBs; Ghirlanda et al. 2004; Li et al. 2008). Hubble parameter $H(z)$, which is defined as $H(z) = \dot{a}/a$, where a denotes the cosmic scale factor and $\dot{a}$ is its rate of change with respect to the cosmic time, is directly related to the expansion history of the Universe. The method based on observational $H(z)$ data (OHD) has been used to test cosmological models (e.g., Yi & Zhang 2007; Chen & Ratra 2011). Besides parameter constraints, OHD can also be used as an auxiliary model selection criterion (Li et al. 2009).

In practice, the Hubble parameter $H(z)$ is usually defined as a function of redshift z, with $a(t)/a(t_0) = 1/(1+z)$, where t_0 is the current cosmic time

$$H(z) = -\frac{1}{1+z}\frac{dz}{dt}\,. \tag{1}$$

∗ Supported by the National Natural Science Foundation of China.

z is the cosmological redshift and t is the age of the Universe when the observed photon is emitted. The derivative of redshift with respect to cosmic time, dz/dt, has a direct effect on $H(z)$. $H(z)$ has been measured through the differential age method according to Equation (1), which was first put forward by Jimenez & Loeb (2002). This differential age method has been demonstrated in Jimenez et al. (2003). However, it may be difficult to select galaxies that can act as "cosmic chronometers" and accurately determining the age of a galaxy by considering stars in a galaxy to be continuously born, since a young stellar population dominates their emission spectra (Zhang et al. 2010). Luminous red galaxies (LRGs) which have photometric properties consistent with an old, passively evolving stellar population (Roseboom et al. 2006) are regarded as good candidates to act as "cosmic chronometers" (Crawford et al. 2010).

We employ ULySS[1], an available online package used to fit a full-length spectrum. As the relatively homogeneous stellar component of LRGs, we use single stellar population (SSP) fitting and gain age information, which will be discussed in detail in Section 3. With the age-redshift relation, four OHD points are deduced accordingly.

There are already 21 OHD points obtained from both the differential age method (Jimenez et al. 2003; Simon et al. 2005; Stern et al. 2010; Moresco et al. 2012) and the BAO method (Gaztañaga et al. 2009). Currently the number of OHD points is still small compared with SNIa luminosity distance data. The potential power of OHD in constraining cosmological parameters is explored in Ma & Zhang (2011) in detail. They conclude that the constraining power of OHD can be as strong as that of SNIa when its quantity reaches a certain value, which is 64 based on the error model used in that paper, thus it is worthwhile to acquire new independent measurements for the Hubble parameter.

This paper is organized as follows. We briefly describe the selection of our sample of LRGs in Section 2. In Section 3, we explain how we derive information about the age from LRG spectra using ULySS and in Section 4 we present our method to obtain the OHD from galaxy ages. A cosmology constraint using all available OHD including our four new ones is given in Section 5. Finally, in the last section, we discuss the limitations and prospects of our results.

2 SOURCE SELECTION FOR OUR SAMPLE OF LRGS

It is important and necessary to select a large homogeneous passively evolving sample of LRGs to obtain the age-redshift relation. The Sloon Digital Sky Survey (SDSS) (York et al. 2000; Stoughton et al. 2002; Abazajian et al. 2003) is currently the largest photometric and spectroscopic sky survey, which includes five-band images over 10^4 deg^2 with accurate photometric calibration and spectroscopy of 10^6 galaxies (Abazajian et al. 2009). The SDSS spectroscopic survey consists of two samples of galaxies selected with different criteria, which are named the MAIN sample (Strauss et al. 2002) and the LRG sample (Eisenstein et al. 2003) respectively. The wavelengths for these galaxy spectra range from 3800 Å to 9200 Å with spectral resolution $\lambda/(\Delta\lambda)$ = 1850–2200. Using dedicated software, the SDSS project has calibrated the spectral flux, and converted the reference and spectra to the heliocentric frame and the vacuum wavelengths respectively.

We chose the sample by applying LRG selection criteria given by SDSS Data Release 7 (DR7) which are: (i) Selecting galaxies from the Catalog Archive Server (CAS) database with the TARGET_GALAXY_RED flag. (ii) The signal-to-noise ratio (S/N) of the r-waveband should be greater than 10. (iii) The restrictions should satisfy specClass = 'SPEC_GALAXY', zStar = 'XCORR_HIC', zWarning = 0, eClass $<$ 0, z $<$ 0.4 and fracDev_r $>$0.8. The LRG selection criteria of SDSS (Eisenstein et al. 2001) are based on the color and magnitude to yield a sample of luminous, intrinsically red galaxies. However, the sample selected from SDSS according to Eisenstein's selection criteria is not very homogeneous. Furthermore, we use the sample from Carson & Nichol (Carson & Nichol 2010) with a constraint on S/N. As S/N has an impact on our next fitting step, it is necessary to demand S/N in the R-band to be greater than 10. 17 832 selected

[1] ULySS is available at: *http://ulyss.univ-lyon1.fr/*

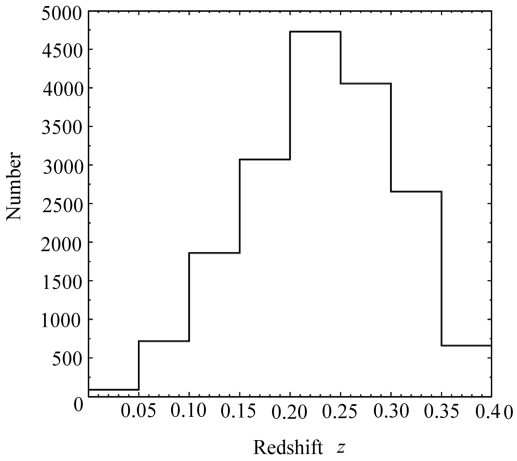

Fig. 1 Redshift distribution of 17 832 LRGs.

quiescent, luminous red galaxies based on the Carson & Nichol sample method from SDSS DR7 cover the redshift range from 0–0.4. The redshift distribution of our sample is shown in Figure 1.

Compared to other works where LRGs are selected based on spectra, the Carson & Nichol sample calibrates, for the first time, the SDSS spectra on the Lick/Image Dissector Scanner system. Their general selection criteria are as follows. First obtain LRGs from CAS as outlined in Eisenstein et al. (2001). Constrain the spectrum using standard emission lines such as Hα, Hβ and OIII 5007 to increase the number of truly quiescent galaxies. To fully picture physical properties such as velocity dispersion and absolute luminosity of these LRGs, through correcting velocity dispersions for aperture effects and performing $K + e$ corrections to the magnitude, four subsamples are produced with different absolute magnitudes and velocity dispersions. For an explicit description of this method, please refer to Carson & Nichol (2010).

3 AGE-REDSHIFT RELATION

We proceed to describe our way of obtaining age information for LRGs. There are many methods to find the age and metallicity of stellar systems from a spectrum, such as SED fitting, spectrophotometric indices (e.g., Lick, Rose indices) and full spectrum fitting (Koleva et al. 2008). In this paper, we adopt the full spectrum fitting method to analyze the physical properties of stellar populations. Full spectrum fitting, which makes use of all the information contained in the signal, is insensitive to extinction or flux calibration errors and independent of the shape of the continuum. We adopt the open-source software package, ULySS, to explore the history of stellar populations.

ULySS is a full spectrum fitting package developed by a group at the Université de Lyon (Koleva et al. 2009b). Its goal is to seek the minimum χ^2 in the process of fitting an observed spectrum with a model spectrum in the pixel space with the MPFIT function. When fitting the observed spectrum ($F_{\rm obs}(\lambda)$), the package uses a linear combination of k non-linear components (CMP$_i$) with weights W_i to approximate it. In this process, the composite model is possibly convolved with a line-of-sight velocity distribution (LOSVD), multiplied by an $n^{\rm th}$ order polynomial $P_n(\lambda)$ and summed with another polynomial $Q_m(\lambda)$ (for more details please refer to Koleva et al. 2009b)

$$F_{\rm obs}(\lambda) = P_n(\lambda) \times \{{\rm LOSVD}(v_{\rm sys}, \sigma, h3, h4) \otimes \sum_{i=0}^{i=k} W_i {\rm CMP}_i(a_1, a_2, a_3, ..., \lambda)\} + Q_m(\lambda). \quad (2)$$

For the study of a stellar population, the CMP_i is characterized by age and [Fe/H]. It uses the Levenberg-Marquardt routine to evaluate parameters in individual CMP_i and the coefficients of $P_n(\lambda)$ and $Q_m(\lambda)$ (Koleva et al. 2009b). This method has already been successfully tested in Wu et al. (2011). The reliability and robustness of using ULySS for the study of the history of a stellar population has been verified (e.g., Koleva et al. 2009c,a).

3.1 Model Selection and Matching Resolution

There are several population models and in our paper, and three of them are provided by the package ULySS: Pegase-HR/ELODIE3.1, Galaxev/STELIB (hereafter BC03) and Vazdekis/Miles. The information about these models is listed in Table 1. Koleva et al. (2008) also test these three models and verify their reliability.

Table 1 Information on the Three Models

Model	Library	Resolution (Å)	Wavelength (Å)	Age (Gyr)	[Fe/H] (dex)	IMF
Pegase	ELODIE3.1	0.55	$4000-6800$	$0.1-20$	$-3.21-1.62$	Salpeter
Galaxev	STELIB	3	$3200-9500$	$0.1-20$	$-2.3-0.4$	Chabrier
Vazdekis	MILES	2.3	$3525-7500$	$0.1-17.5$	$-1.7-0.2$	Salpeter

The full spectrum fitting uses the redundancy of the spectrum and the multiplicative polynomial could decrease the influence of flux calibration and Galactic extinction. On the other hand, the fitting method is more sensitive to the wavelength range of the spectrum. The spectra from SDSS span the wavelengths from 3800 Å to 9200 Å, but as we can see, only the wavelength range of BC03 could cover the whole wavelength of spectra from SDSS. After comparison of the three different models, we choose BC03 as a reliable model to use.

The first step in fitting is to match resolutions between the observed spectra with the model we chose. There are two ways for matching, either by transforming the resolution of the model or the observed spectrum. In our paper, we choose to transform the model provided by ULySS by including a relative line spread function (LSF) between our spectrum and the model. When determining the LSF, we make use of the template stars, available from *http://www.sdss.org/dr7/algorithms/veldisp.html* as standard stars. We perform a fifth order linear interpolation in wavelength and convolve with the model. In this way, a new matching model is generated, and this whole process can be accomplished through functions in ULySS (Koleva et al. 2009b).

3.2 Single Stellar Population Fit

It is essential to study the stellar population of galaxies if we want to reconstruct their star formation history. We fit the spectrum with an SSP for the following reasons. Firstly, LRGs are believed to be drawn from the same parent population with the largest fraction of their stars being formed from a single burst. Secondly, SSPs that show equivalent properties correspond to a "luminosity weighted" average over the distributions. Thus with a single SSP fitting, a general view of a galaxy can be obtained (Du et al. 2010). We carry out an initial study of age-dating using the stellar population models of Bruzual & Charlot (2003); Stern et al. (2010) to synthesize spectra, a process which is also provided by ULySS.

But when interpreting the galaxy spectra, we find that the initial values of both age and metallicity tend to affect the fitting result. It is difficult to remove such influences, especially in low resolution spectra (Du et al. 2010). The fitting provided by ULySS starts from a point (initial value) in the parameter space (age and metallicity), therefore we emphasize the importance of this point in the fitting process which may only find a local minimum. In order to identify and understand the age-metallicity degeneracy and effects of local minimizations, we analyze the age-metallicity

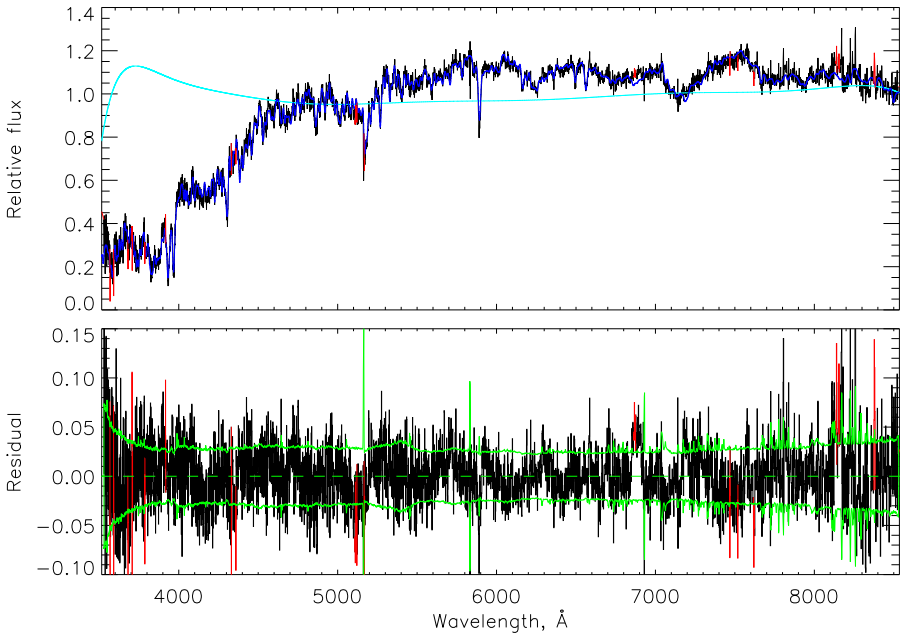

Fig. 2 Best fit with the BC03 model and the residual spectrum for a galaxy. The top panel shows the spectrum in black and the best fit in blue. The red regions are rejected from the fit and the indigo line is the multiplicative polynomial. The bottom panel shows the residuals from the best fit. The continuous green lines represent the 1σ deviation. The dashed green line shows a residual value of zero.

degeneracy and construct a χ^2 map, which is a function provided by ULySS. The χ^2 map is a visualization of parameter space, and the goal of this map is to give a grid of nodes in a 2-D projection of the parameter space. The χ^2 map returns the minimization of each node (Koleva et al. 2009b). A subsample of 164 LRG spectra from redshift 0.03 to 0.179 is processed by building their χ^2 maps. It has been discovered that the metallicity of LRGs are consistent with the assumption that selected galaxies are thought to have similar metallicities (Jimenez et al. 2003) which range between about 0.1 dex and 0.2 dex.

ULySS can provide various points in the parameter space as initial values, that is to say, if the number of points is sufficient, it is possible to find the global minimization and thus break the degeneracy. We set the range of our metallicity to be 0.1–0.2 dex for every galaxy in our sample, while the range for age is from 5000–11 200 Myr. Figure 2 shows the best fit with the BC03 model and the residual spectrum for a galaxy when a specific group of initial values is given.

For each galaxy, groups of age and metallicity values can be collected as results. We ignore the metallicity and just focus on age. To identify accurate values for the age of each galaxy, we base our selections on the minimal χ^2 criterion. In particular, if all fitted ages for a single galaxy exceed the age of our Universe, it is not acceptable. There are several reasons that can cause this situation, such as low resolution of spectra and model dependence. In the fitting process, we set a limit such that $a + \sigma < 16$ Gyr, where a is the fitting age and σ is the error, to exclude the situation where the age of a galaxy exceeds the age of the Universe. The fitting result is shown in Figure 3. For clarity, ages less than 7 Gyr have not been plotted. In this figure, a clear trend that the ages of galaxies decrease with the redshift is displayed.

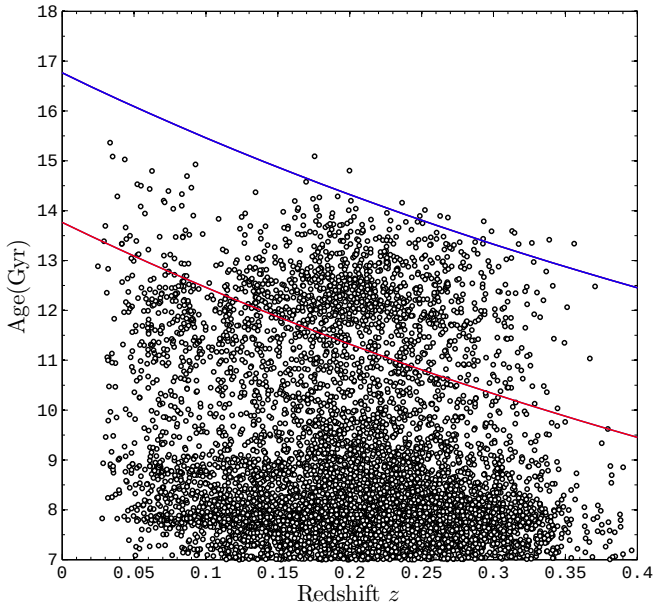

Fig. 3 Fitting results of the 17 832 LRGs. For clarity, the ages less than 7 Gyr have not been plotted. The lower line shows the theoretical age of the Universe $t(z)$ for a ΛCDM model with $\Omega_m = 0.29$ and $H_0 = 69$ km s^{-1} Mpc^{-1}. The upper line indicates $t(z) + 3$ Gyr, where the 3 Gyr comes from the systematic errors. A clear trend is present: the oldest ages of the galaxies decrease with redshift.

4 THE DETERMINATION OF OHD

According to Equation (1), the slope of the linear fit of $t(z_i)$, which is the oldest age at redshift z_i, is directly related to the Hubble parameter. That is, the Hubble parameter at $z_{\rm eff}$, $H(z_{\rm eff})$, can be calculated by formula $H(z_{\rm eff}) = -[1/(1+z_{\rm eff})](\Delta t/\Delta z)^{-1}$, where $z_{\rm eff} = (z_{\rm max} + z_{\rm min})/2$.

Mathematically, the value of $\Delta z = z_{\rm max} - z_{\rm min}$ should not be too large, so we divide our data into four redshift regions, $0.03 \leq z \leq 0.11$, $0.08 \leq z \leq 0.16$, $0.16 \leq z \leq 0.24$ and $0.24 \leq z \leq 0.32$.

To calculate $t(z_i)$ for each subsample, we adopt a common bin-dividing method. Take the first subsample for example. We divide it into several bins from 3 to 20, select the oldest galaxy from each bin as a set of $t(z_i)$ and fit the corresponding points of $t(z_i)$ with a straight line to get a candidate of OHD in this subsample. Here we get 18 candidates of OHD in this subsample. The number of bins corresponding to the selected candidate is called $n_{\rm best}$. Three parameters are used here for selecting the most suitable number of bins that we choose: SSE$/n$ for the mean squared error where SSE is the sum of squared error, $\sigma_{\rm slope}/{\rm slope}$ for the relative error in the fitting result of the slope and $P_{\geq \chi^2}$ for the goodness of fit. The remaining subsamples follow the same method.

Here we explain our reason for choosing the above three parameters as the criteria. Imagine that a line that defines an envelop can be obtained naturally with ideal data, therefore, we should take the number of bins n to be as large as possible. Unfortunately, for the real case, the envelop strongly fluctuates. This is due to the existence of "fake-oldest galaxies," which formed too late to be considered as a "cosmic chronometer" compared with the LRGs at other redshifts. Therefore, large n would increase the risk of selecting the "fake-oldest galaxies" as a "cosmic chronometer." That is what the parameter SSE$/n$ can indicate, with value 0 representing the ideal case. Conversely,

too small n represents large statistical errors, which are evaluated by the parameter $\sigma_{\rm slope}/{\rm slope}$. Moreover, $P_{\geq\chi^2}$ is calculated to represent the goodness of fit. Taking the three parameters into account, we finally obtain the value of $n_{\rm best}$ for each subsample.

In every subsample, we expect the $n_{\rm best}$ satisfies the smallest SSE$/n$, the largest $P_{\geq\chi^2}$ and the smallest absolute value of $\sigma_{\rm slope}/{\rm slope}$. In the first subsample, the $n = 6$ case satisfies the criterion perfectly, as does $n = 7$ in the second subsample and $n = 6$ in the third subsample. For the fourth case, judging the $\sigma_{\rm slope}/{\rm slope}$ first, we can see that both $n = 10$ and $n = 12$ share the smallest value. Then, considering the second parameter SSE$/n$, we chose $n = 12$ for a smaller value. Besides, its $P_{\geq\chi^2}$ is also satisfied.

Figure 4 shows the oldest ages in each bin when we divide the subsamples into their corresponding $n_{\rm best}$ bins and their optimal fits are also plotted. We will next introduce how we derive the best parameters for linear fitting and their error bars.

When we fit n sets of data (z_i, t_i) with a straight line $t = kz + b$ and the error of t_i is σ_i ($i = 1, 2, ..., n$), the best parameters for the linear fitting are obtained by minimizing the χ^2

$$\chi^2 = \sum_{i=1}^{n} \frac{(t_i - kz_i - b)^2}{\sigma_i^2}\,. \tag{3}$$

To get the error for σ_k, we must rewrite Equation (3) as follows so that we can estimate errors for the regression parameters

$$\chi^2 = \sum_{i=1}^{n} \left(\frac{t_i}{\sigma_i} - k\frac{z_i}{\sigma_i} - b\frac{1}{\sigma_i}\right)^2. \tag{4}$$

This form of χ^2 is the same as that when we fit the data of (t_i/σ_i,z_i/σ_i, $1/\sigma_i$) with a linear function of $\frac{t}{\sigma} = k\frac{z}{\sigma} + b\frac{1}{\sigma}$ with the same method for minimizing χ^2.

Then, using the well known formula for confidence intervals of regression coefficients at a confidence level of $1 - \alpha$ (seeing any textbook on regression such as He & Liu 2011, for details), we can get the error of k which can be regarded as σ_k (i.e. $\sigma_{\rm slope}$ in Table 2)

$$\sigma_k = \sigma_{\rm slope} = |t_{(\alpha/2,\ n-2)}|\sqrt{\frac{S(1,1)}{n-2} \times {\rm SSE}}\,, \tag{5}$$

where $|t_{(\alpha/2,\ n-2)}|$ is the absolute value of the inverse of Student's t Cumulative Distribution Function with $n - 2$ degrees of freedom for the corresponding probabilities in $\alpha/2$, which can be calculated with function of tinv in MATLAB and the $S(1, 1)$ is the element in the first row and first column in the inverse of the following matrix

$$\begin{pmatrix} \sum\limits_{i=1}^{n} \frac{z_i^2}{\sigma_i^2} & \sum\limits_{i=1}^{n} \frac{z_i}{\sigma_i^2} \\ \sum\limits_{i=1}^{n} \frac{z_i}{\sigma_i^2} & \sum\limits_{i=1}^{n} \frac{1}{\sigma_i^2} \end{pmatrix}. \tag{6}$$

In addition, the steps above can be easily performed by MATLAB Toolboxes.

With Equation (1), we can get the relation between the error of $H(z)$ and $\sigma_{\rm slope}$

$$\sigma_H = \frac{1}{1 + z_{\rm eff}} \frac{1}{\sigma_{\rm slope}^2}\,, \tag{7}$$

with which the error of $H(z)$ is finally calculated.

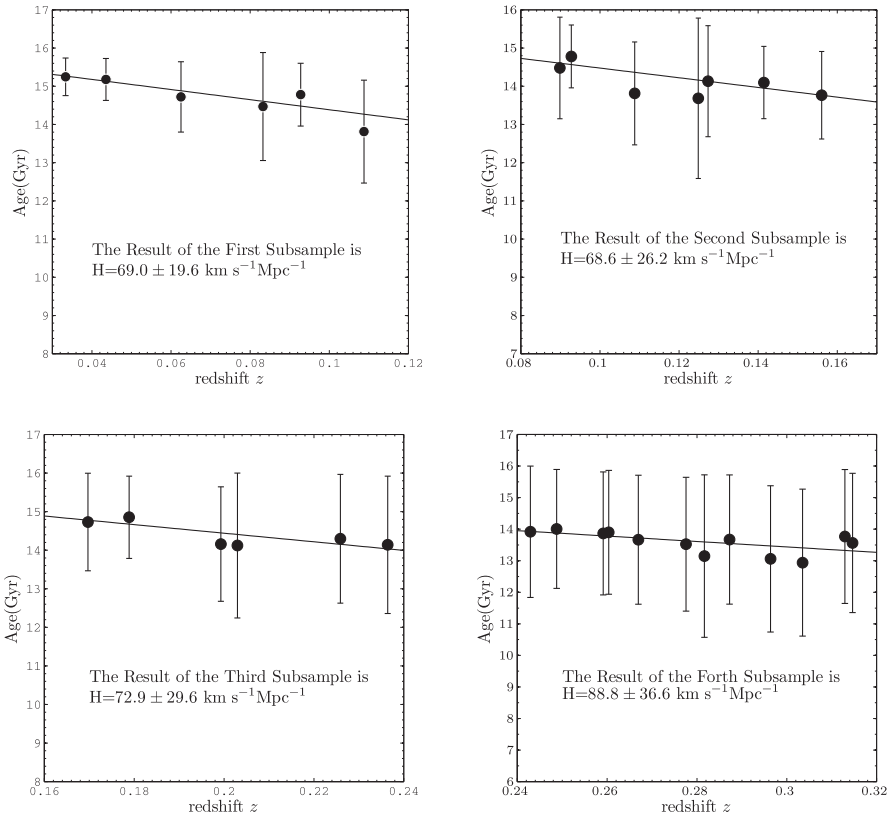

Fig. 4 The oldest ages in each bin when we divide the subsamples into their corresponding $n_{\rm best}$ bins and their optimal fitted results. The solid line represents the best fitting for each subsample. In the first subsample, $z_{\rm min} = 0.033$, $z_{\rm max} = 0.109$ and $z_{\rm eff} = 0.07$. In the second subsample, $z_{\rm min} = 0.090$, $z_{\rm max} = 0.156$ and $z_{\rm eff} = 0.12$. In the third subsample, $z_{\rm min} = 0.170$, $z_{\rm max} = 0.236$ and $z_{\rm eff} = 0.20$, and in the forth subsample, $z_{\rm min} = 0.243$, $z_{\rm max} = 0.315$ and $z_{\rm eff} = 0.28$.

Table 2 Fitting Results

n	4	5	6	7	8	5	6	7	8	9
$-\sigma_{\rm slope}$/slope	0.64	0.44	0.28	0.31	0.28	0.49	1.45	0.38	0.54	0.74
SSE/n	0.053	0.076	0.049	0.106	0.094	0.251	0.964	0.319	0.802	1.575
$P_{\geq\chi^2}$†	0.900	0.945	0.990	0.980	0.993	0.969	0.915	0.997	0.992	0.980
n	4	5	6	7	8	10	11	12	13	14
$-\sigma_{\rm slope}$/slope	1.08	0.43	0.41	0.50	0.44	0.41	0.43	0.41	0.43	0.43
SSE/n	0.028	0.019	0.017	0.034	0.031	0.208	0.113	0.175	0.163	0.211
$P_{\geq\chi^2}$†	0.945	0.992	0.999	0.999	0.999	1.000	1.000	1.000	1.000	1.000

Notes: † Too large of $P_{\geq\chi^2}$ values in these two subsamples result from too large of errors. The two other parameters are taken into account mainly because of the very close $P_{\geq\chi^2}$ in this subsample.

5 COSMOLOGICAL CONSTRAINTS FROM OHD

Now we have a total of 25 available OHD which are listed in Table 3 and plotted in Figure 5. Using these 25 OHD, we constrain the cosmological parameters. The best fit parameters of the model via

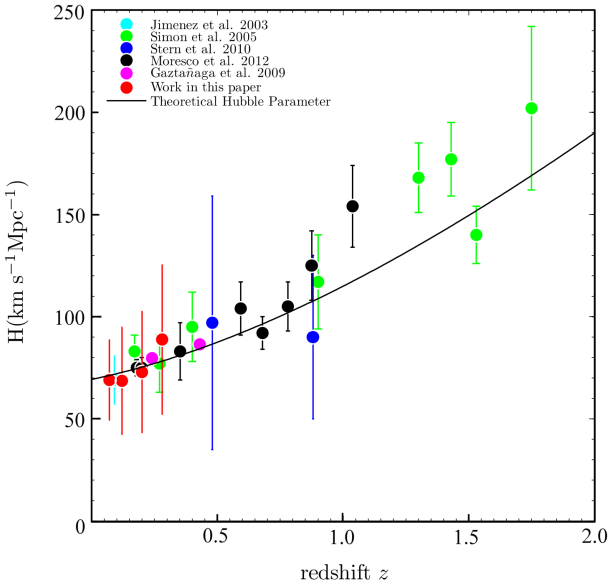

Fig. 5 All available OHD points. The solid line plots the theoretical Hubble parameter $H_{\rm fid}$ as a function of z from the spatially flat ΛCDM model with $\Omega_m = 0.3$, $\Omega_\Lambda = 0.7$ and H_0 = 72 km s^{-1} Mpc^{-1}. The OHD points are listed in Table 3.

OHD are determined by minimizing the χ^2

$$\chi^2_{\rm OHD}(\boldsymbol{p}_{\rm model}) = \sum_{i=1}^{N} \frac{(H_{\rm obs}(z_i) - H_{\rm th}(z_i))^2}{\sigma^2_{{\rm obs},i}}, \tag{8}$$

where $\boldsymbol{p}_{\rm model}$ is a vector of free parameters. Based on the basic equations defining the ΛCDM model, we have the following two models: for a flat ΛCDM ($\Omega_k = 0$),

$$H_{\rm th}(z) = H_0\sqrt{\Omega_m(1+z)^3 + (1-\Omega_m)} \qquad \text{with} \quad \boldsymbol{p}_{\rm flat} = (\Omega_m, H_0);$$

for a non-flat ΛCDM,

$$H_{\rm th}(z) = H_0\sqrt{\Omega_m(1+z)^3 + \Omega_\Lambda + (1-\Omega_\Lambda-\Omega_m)(1+z)^2},$$

with $\boldsymbol{p}_{\rm non-flat} = (\Omega_\Lambda, \Omega_m, H_0)$. For both models, the likelihood function can be written as $L \propto \exp(-\chi^2_{\rm OHD}/2)$.

We use the MCMC method to calculate the likelihood in the independent parameter space. Markov chains are generated and analyzed via the Python MCMC code – `Pymc`. The parameter H_0 and the density parameter $\boldsymbol{\Omega} = (\Omega_m,\ \Omega_\Lambda)$ are treated as independent parameters in these two models (Wei 2010), and all of their prior distributions are set to be a uniform distribution (Table 4).

Figures 6 and 7 show the one-dimensional marginalized probability distribution for each parameter in the diagonal entries and the two-dimensional marginalized confidence regions in the off-diagonal entries of the flat ΛCDM model and non-flat ΛCDM model respectively. The respective confidence regions ($68.7\%,\ 95.45\%,\ 99.73\%$) for each parameter are calculated. The best fit parameters are indicated in the contour plots with vertical and horizontal lines.

To compare the results of constraining the "new version OHD" with the results of adding the new points we obtained in this paper and the "old version OHD" (see Table 3 for details), we display

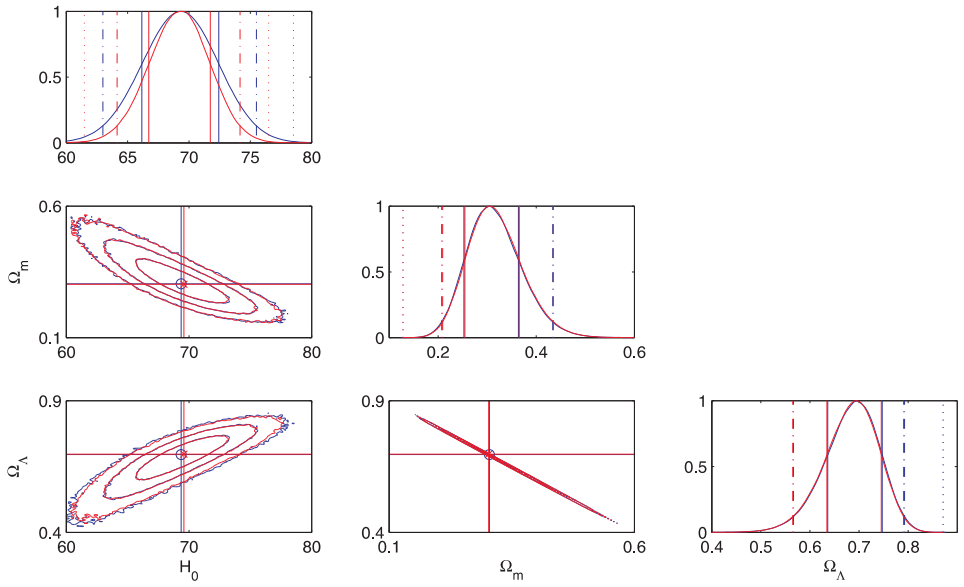

Fig. 6 OHD constraint region for flat ΛCDM. Red lines represent the "new version" of OHD and the blue ones denote the "old version." The plots along the diagonal show the 1-D probability density function (PDF) and the vertical lines from center to edge show the respective confidence intervals; The plots that are off the diagonal show the 2-D confidence regions with inner and outer contours denoting the respective confidence levels. The open blue circles indicate the best fit point by the "old version" while the red crosses show the ones from the "new version."

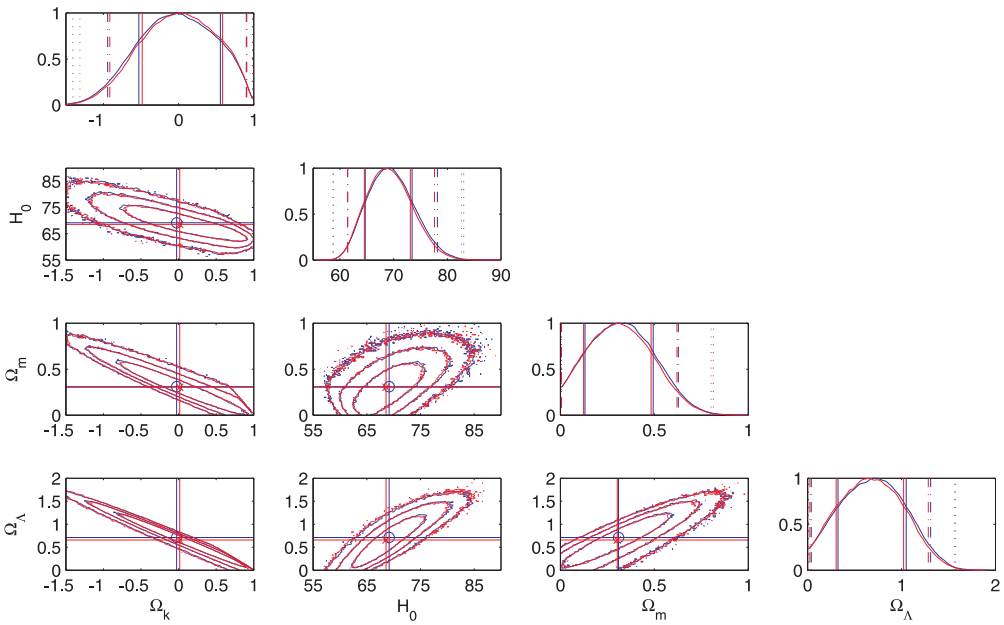

Fig. 7 Same as Fig. 6 except for non-flat ΛCDM.

Table 3 All Available OHD

z	$H(z)^{\dagger}$	$\sigma_{H(z)^{\dagger}}$	Reference
0.090	69	12	Jimenez et al. (2003)
0.170	83	8	Simon et al. (2005)
0.270	77	14	Simon et al. (2005)
0.400	95	17	Simon et al. (2005)
0.900	117	23	Simon et al. (2005)
1.300	168	17	Simon et al. (2005)
1.430	177	18	Simon et al. (2005)
1.530	140	14	Simon et al. (2005)
1.750	202	40	Simon et al. (2005)
0.480	97	62	Stern et al. (2010)
0.880	90	40	Stern et al. (2010)
0.179	75	4	Moresco et al. (2012)
0.199	75	5	Moresco et al. (2012)
0.352	83	14	Moresco et al. (2012)
0.593	104	13	Moresco et al. (2012)
0.680	92	8	Moresco et al. (2012)
0.781	105	12	Moresco et al. (2012)
0.875	125	17	Moresco et al. (2012)
1.037	154	20	Moresco et al. (2012)
0.24	79.69	3.32	Gaztañaga et al. (2009)
0.43	86.45	3.27	Gaztañaga et al. (2009)
0.07	69.0	19.6	††
0.12	68.6	26.2	††
0.20	72.9	29.6	††
0.28	88.8	36.6	††

† The unit is km s^{-1} Mpc^{-1}. †† Work in this paper.

Table 4 The Prior Used for Model Parameters

Model Parameters	Prior Distribution
Ω_m	Uniform (0.0,1.5)†
Ω_Λ	Uniform (0.0, 2.5)†
H_0	Uniform (50, 100)†

† *Uniform (lower limit, upper limit)* stands for a uniform distribution in the interval [lower limit,upper limit].

both results in Figures 6 and 7 with different colored lines to distinguish them: the red lines refer to the "new version OHD" and the blue ones denote the "old version OHD."

The constraints in Figures 6 and 7 show the good performances in constraining ΛCDM. In Figures 6 and 7 the 1-D marginalized constraints are more stringent than the old one and for the same model the contour plots against the same pair of parameters have a smaller region at the same level of confidence. Since the number of newly added points is small, the amount of shrinkage is also small.

6 CONCLUSIONS AND DISCUSSION

In this paper, we present our measurements of four new OHD data points from the ages of passively-evolving galaxies at redshift $0 < z < 0.4$. A large sample of spectra from LRGs has been fitted by us with SSP models and an age-redshift relation is obtained and displayed. By computing the relative ages of these LRGs, we gain four new OHD data points. Combining them with 21 other available OHD points, we constrain cosmological parameters using the updated dataset of OHD. It should

be mentioned that similar work (Liu et al. 2012) used the SDSS DR7 to constrain H_0, a particular value of the Hubble parameter at $z = 0$. We hope to give a tighter constraint on cosmology parameters with our new OHD data points. Unfortunately, these four points give limited improvements for constraining cosmological parameters more accurately, because of the relatively large error bars associated with these points.

Here, we explain the possible reasons. Firstly, the low S/N of the spectra from SDSS leads to a large uncertainty when calculating the age of the galaxies. Combining spectra from various observational project may be a solution, as discussed in Jimenez et al. (2003); Stern et al. (2010). Comparing our points with previous ones, especially those in Simon et al. (2005) and Moresco et al. (2012), although there is a large difference in terms of accuracy, we would like to illustrate the following. One is a theoretically good method to obtain the age of an LRG in Moresco et al. (2012). Still, there are many problems in the method that need to be solved. The other is that the results from Simon et al. (2005) are more accurate than ours because of the high quality of their spectra. OHD in Stern et al. (2010), whose quality of spectra and method of fitting spectra are similar to ours, share a comparable degree of accuracy with us, which also demonstrates the objectivity of our OHD.

Second, as our selected LRGs are incomplete and unable to cover all old galaxies in the Universe, there could be some difficulty in tracing the "cosmic chronometers." That is to say, the oldest age in our sample may not represent cosmic age at that redshift. This should be improved through future redshift surveys and lead to successful realization of the differential age method. In addition, as high S/N is essential for a precise fitting which determines the age of galaxies, we suggest that the accuracy of OHD would be improved if the S/N of spectra increases. We employ ULySS to reconstruct the stellar population of galaxies. Though the robustness of ULySS has been illustrated, the fitting may still be a local minimum because of the limitation of good initial values. There has been significant advancement in modeling stellar populations of LRGs and we expect these to improve the accuracy of this process in the future.

The number of OHD is still small compared with SNIa data sets. The advantages of constraining cosmological models with OHD (Jimenez & Loeb 2002; Maor et al. 2001) have been demonstrated, therefore increasing the number of OHD is imperative. OHD play almost the same role as that of SNIa for the joint constraints on the ΛCDM model. The number of OHD points will be extended in further decades with more and deeper observations of galaxies and at that time the OHD set alone will be capable to be used in place of current SNIa data sets (Ma & Zhang 2011). Fortunately, we have seen that the proposed observational plan to conduct a Sandage-Loeb test (Corasaniti et al. 2007) can be used to extend our knowledge of cosmic expansion into an even deeper redshift. Finally, we think it is reasonable to expect that OHD will complement SNIa, BAO and weak lensing and help us derive more information about the evolution history of our Universe.

Acknowledgements Special thanks go to Robert C. Nichol and Dan P. Carson for providing us the LRG sample data. We are grateful to G. Bruzual, M. Koleva, Wei Du, Gao-Chao Liu, Xian-Min Meng, Xue-Lei Chen, You-Jun Lu and Cong Ma for their helpful suggestions. This work was supported by the National Natural Science Foundation of China (Grant No. 11173006), the National Basic Research Program of China (973 Program, 2012CB821804) and the Fundamental Research Funds for the Central Universities.

References

Abazajian, K., Adelman-McCarthy, J. K., Agüeros, M. A., et al. 2003, AJ, 126, 2081
Abazajian, K. N., Adelman-McCarthy, J. K., Agüeros, M. A., et al. 2009, ApJS, 182, 543
Bruzual, G., & Charlot, S. 2003, MNRAS, 344, 1000
Carson, D. P., & Nichol, R. C. 2010, MNRAS, 408, 213
Chen, Y., & Ratra, B. 2011, Physics Letters B, 703, 406

Corasaniti, P.-S., Huterer, D., & Melchiorri, A. 2007, Phys. Rev. D, 75, 062001
Crawford, S. M., Ratsimbazafy, A. L., Cress, C. M., et al. 2010, MNRAS, 406, 2569
Du, W., Luo, A. L., Prugniel, P., Liang, Y. C., & Zhao, Y. H. 2010, MNRAS, 409, 567
Eisenstein, D. J., Annis, J., Gunn, J. E., et al. 2001, AJ, 122, 2267
Eisenstein, D. J., Hogg, D. W., Fukugita, M., et al. 2003, ApJ, 585, 694
Eisenstein, D. J., Zehavi, I., Hogg, D. W., et al. 2005, ApJ, 633, 560
Gaztañaga, E., Cabré, A., & Hui, L. 2009, MNRAS, 399, 1663
Ghirlanda, G., Ghisellini, G., Lazzati, D., & Firmani, C. 2004, ApJ, 613, L13
He, X., & Liu, W. 2011, Applied Regression Analysis (China Renmin University Press)
Hicken, M., Wood-Vasey, W. M., Blondin, S., et al. 2009, ApJ, 700, 1097
Jimenez, R., & Loeb, A. 2002, ApJ, 573, 37
Jimenez, R., Verde, L., Treu, T., & Stern, D. 2003, ApJ, 593, 622
Koleva, M., de Rijcke, S., Prugniel, P., Zeilinger, W. W., & Michielsen, D. 2009a, MNRAS, 396, 2133
Koleva, M., Prugniel, P., Bouchard, A., & Wu, Y. 2009b, A&A, 501, 1269
Koleva, M., Prugniel, P., De Rijcke, S., et al. 2009c, Astronomische Nachrichten, 330, 960
Koleva, M., Prugniel, P., Ocvirk, P., Le Borgne, D., & Soubiran, C. 2008, MNRAS, 385, 1998
Komatsu, E., Smith, K. M., Dunkley, J., et al. 2011, ApJS, 192, 18
Li, H., Xia, J.-Q., Liu, J., et al. 2008, ApJ, 680, 92
Li, M., Li, X.-D., Wang, S., & Zhang, X. 2009, J. Cosmol. Astropart. Phys., 6, 036
Liu, G., Lu, Y., Chen, X., et al. 2012, ApJ, 758, 107
Ma, C., & Zhang, T.-J. 2011, ApJ, 730, 74
Maor, I., Brustein, R., & Steinhardt, P. J. 2001, Physical Review Letters, 86, 6
Moresco, M., Cimatti, A., Jimenez, R., et al. 2012, J. Cosmol. Astropart. Phys., 8, 006
Percival, W. J., Reid, B. A., Eisenstein, D. J., et al. 2010, MNRAS, 401, 2148
Riess, A. G., Filippenko, A. V., Challis, P., et al. 1998, AJ, 116, 1009
Roseboom, I. G., Pimbblet, K. A., Drinkwater, M. J., et al. 2006, MNRAS, 373, 349
Simon, J., Verde, L., & Jimenez, R. 2005, Phys. Rev. D, 71, 123001
Spergel, D. N., Bean, R., Doré, O., et al. 2007, ApJS, 170, 377
Stern, D., Jimenez, R., Verde, L., et al. 2010, J. Cosmol. Astropart. Phys., 2, 008
Stoughton, C., Lupton, R. H., Bernardi, M., et al. 2002, AJ, 123, 485
Strauss, M. A., Weinberg, D. H., Lupton, R. H., et al. 2002, AJ, 124, 1810
Wei, H. 2010, Physics Letters B, 687, 286
Wu, Y., Singh, H. P., Prugniel, P., Gupta, R., & Koleva, M. 2011, A&A, 525, A71
Yi, Z.-L., & Zhang, T.-J. 2007, Modern Physics Letters A, 22, 41
York, D. G., Adelman, J., Anderson, J. E., Jr., et al. 2000, AJ, 120, 1579
Zhang, T.-J., Ma, C., & Lan, T. 2010, Advances in Astronomy, 2010, 184284